Acta Crystallographica Section A
Foundations of Crystallography
ISSN 0108-7673

Received 13 March 2011
Accepted 18 April 2011

Addressing the amorphous content issue in quantitative phase analysis: the certification of NIST standard reference material 676a

James P. Cline,[a]* Robert B. Von Dreele,[b] Ryan Winburn,[c] Peter W. Stephens[d] and James J. Filliben[a]

[a]National Institute of Standards and Technology, Gaithersburg, MD 20899, USA, [b]Argonne National Laboratory, Argonne, IL 60439, USA, [c]Minot State University, Minot, ND 58707, USA, and [d]Stony Brook University, Stony Brook, NY 11794, USA. Correspondence e-mail: jcline@nist.gov

A non-diffracting surface layer exists at any boundary of a crystal and can comprise a mass fraction of several percent in a finely divided solid. This has led to the long-standing issue of amorphous content in standards for quantitative phase analysis (QPA). NIST standard reference material (SRM) 676a is a corundum (α-Al_2O_3) powder, certified with respect to phase purity for use as an internal standard in powder diffraction QPA. The amorphous content of SRM 676a is determined by comparing diffraction data from mixtures with samples of silicon powders that were engineered to vary their specific surface area. Under the (supported) assumption that the thickness of an amorphous surface layer on Si was invariant, this provided a method to control the crystalline/amorphous ratio of the silicon components of 50/50 weight mixtures of SRM 676a with silicon. Powder diffraction experiments utilizing neutron time-of-flight and 25 keV and 67 keV X-ray energies quantified the crystalline phase fractions from a series of specimens. Results from Rietveld analyses, which included a model for extinction effects in the silicon, of these data were extrapolated to the limit of zero amorphous content of the Si powder. The certified phase purity of SRM 676a is 99.02% $\pm$ 1.11% (95% confidence interval). This novel certification method permits quantification of amorphous content for any sample of interest, by spiking with SRM 676a.

1. Introduction

A surface layer possessing some degree of disorder will exist on any crystalline material owing to relaxation of the crystal structure and inclusion of surface reaction products and adsorbed species (typically water). While this layer may only be of the order of a crystallographic unit in thickness, in a finely divided solid it can easily account for more than 1% of the total mass. This is illustrated in Fig. 1 wherein the total volume percentage of amorphous material is shown using a core-shell model for surface layer thicknesses and particle sizes typically encountered in powder samples. For example, a powder with a 0.2 μm particle size and a surface layer thickness of 0.5 nm (the order of a typical lattice parameter) will possess an amorphous content of 0.75%. X-ray scatter from this disordered surface region will not constitute Bragg diffraction. Therefore the diffraction experiment will not address the measurement of this disordered region. This constitutes a bias in the interpretation of the results from a quantitative analysis by powder diffraction methods: the technique measures only the crystalline fraction and cannot access the amorphous components.

The use of powder diffraction on crystalline mixtures dates back some 80 years and remains the principal method used for quantitative phase analysis (QPA). Current data collection and analysis strategies fall into two basic categories: integrated intensity, single-line methods using the reference intensity ratio (RIR) concept, and whole-pattern quantitative Rietveld (1969) analysis (QRA) wherein structural models are incorporated.

Consider a mixture of two crystalline phases α and β, having mass fractions X_α and X_β, respectively. The ratio of the integrated intensity of the strongest, or 100%, peaks in an X-ray diffraction experiment is

$$\frac{I_\alpha}{I_\beta} = \frac{K_\alpha}{K_\beta}\frac{X_\alpha}{X_\beta}, \qquad (1)$$

where the factors K_α and K_β depend on the atomic structure of each phase. Consideration of the ratio of intensities from two

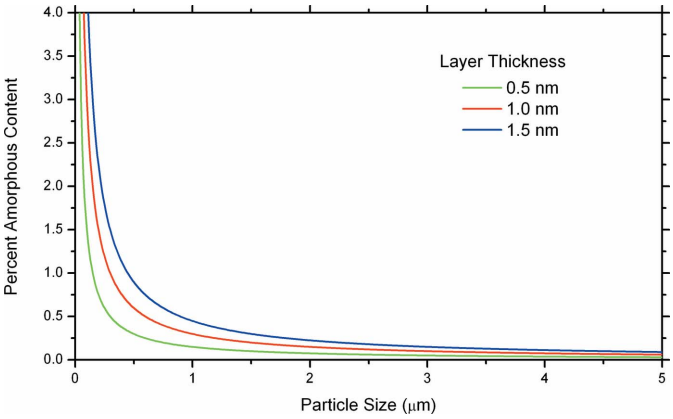

Figure 1
Total amorphous content of a finely divided solid with an amorphous surface layer thickness of approximately 1 to 3 crystallographic units.

phases is much more straightforward than the intensity of either phase alone, as the latter is also dependent on the mass attenuation coefficient of the matrix or sample $(\mu/\rho)_m$, where μ is the linear attenuation coefficient and ρ is the density. The vast majority of phase abundance measurements are performed on laboratory diffractometers of Bragg–Brentano geometry (Klug & Alexander, 1974) wherein the use of intensity ratios as per equation (1) removes the otherwise critical requirement that $(\mu/\rho)_m$ be determined. Chung (1974*a*) referred to the simplification of using intensity ratios as 'matrix flushing'. The use of intensity ratios is the basis of the ubiquitous internal standard method of QPA.

The RIR concept first appeared, implicitly, in Visser & deWolff (1964). The RIR method itself was proposed by Chung (1974*a*,*b*), although he did not refer to it as such. After considerable development by multiple authors, it was effectively summarized by Snyder (1992). He offers the general RIR equation as

$$\mathrm{RIR}_{\alpha,\beta} = \frac{I_\alpha}{I_\beta}\frac{X_\beta}{X_\alpha}, \tag{2}$$

where I_α and I_β are the integrated intensities of the 100% lines for phases α and β, and the X terms are the mass fractions. If a line other than the 100% line is used, an additional relative intensity term is required to scale the intensity of said signature line to the 100% line. In the absence of further information, it is clear that a calibration standard consisting of known ratio by mass of phases α and β must be prepared in order to determine $\mathrm{RIR}_{\alpha,\beta}$. Generalization to more than two phases is straightforward. It can be seen from this discussion that the RIR is a constant relating the diffraction intensities from the two materials in question.

Visser & deWolff (1964) proposed using an RIR value of the phase in question relative to α-alumina (corundum structure), I/I_{corundum}, hereafter abbreviated I/I_c, as a calibration constant. The I/I_c for phase α is defined as

$$\left(\frac{I}{I_c}\right)_\alpha = \frac{I_\alpha}{I_c}\frac{X_c}{X_\alpha} = \frac{I_\alpha}{I_c}\frac{0.5}{0.5} = \frac{I_\alpha}{I_c}, \tag{3}$$

which is, by definition, $\mathrm{RIR}_{\alpha c}$. Thus, the I/I_c constitutes the intensity ratio of the 100% line from a specific phase relative to that of alumina, from a 50/50 mixture, by mass, of the two components.

Chung (1974*b*) proposed what he called an 'adiabatic' method to eliminate the need for a calibration standard mixture. Snyder (1992) later termed it the 'normalized RIR' method. The idea is based on knowing values of reference intensity ratios to some common standard phase s as follows,

$$\frac{X_\alpha}{X_\beta} = \frac{I_\alpha}{I_\beta}\frac{\mathrm{RIR}_{\beta,s}}{\mathrm{RIR}_{\alpha,s}}. \tag{4}$$

This relates the mass ratio of two phases in a mixture to the RIRs of these two phases relative to an arbitrary third phase. If such RIR values are known for all (n) phases in a mixture, then $n-1$ equations of the form of (4) may be generated. The solution of these equations is allowed by the additional assumption

$$\sum_{k=1}^{n} X_k = 1, \tag{5}$$

which says that all of the phases in the mixture are known, and that there is no amorphous component.

The International Centre for Diffraction Data (ICDD), recognizing that inclusion of I/I_c values in the powder diffraction file (PDF) would permit a quantitative analysis without the need to prepare specific calibration standards, began an effort in 1987 to include these data in the PDF. This, in turn, led to the effort at the National Institute of Standards and Technology (NIST) to produce a standard reference material (SRM) optimized for I/I_c determinations. NIST SRM 676 (NIST, 2005), alumina internal standard for quantitative analysis by X-ray powder diffraction, was initially certified in 1992.

The advantage of RIR methods is that the analysis is generally much simpler, as long as the values of the RIR are known for each phase. Disadvantages include the requirement that the chosen signature peak from each phase must not overlap any peaks from any other phase in the sample, preferred orientation can distort the results, and one must be certain to have identified all of the phases in a sample.

With the QRA method (Hill & Howard, 1987; Bish & Howard, 1988), structural models are refined onto the data and used to compute phase abundance. For example, with the Rietveld code *GSAS* (Larson & Von Dreele, 2004),

$$\frac{X_\alpha}{\sum_{k=1}^{n} X_k} = \frac{S_\alpha Z_\alpha w_\alpha}{\sum_{k=1}^{n} S_k Z_k w_k}, \tag{6}$$

where X_α is the mass fraction of crystalline phase α, S_x are the refined scale factors, w_x are the formula weights, Z_x are the number of formula weights per unit cell, and the summations are carried out over the various phases within the mixture. Note that in *GSAS* the scale factors are defined to be proportional to the 'unit cell' fraction; other Rietveld refinement codes may define the scale factor differently. Profile refinement offers the advantage of observing and correcting for preferred orientation, as well as a means to check that all

phases present have been included in the analysis. The requirement that crystal structures of all phases must be known can be overcome by suitable hybrid methods (Madsen & Scarlett, 2008). As with RIR methods, equation (6) can be used only if the assumptions of equation (5) are correct. Therefore, regardless of the method, the technique cannot access the amorphous components directly.

While the diffraction experiment can only access the crystalline material of a sample, the weighing operation used to prepare samples for analysis *via* the internal standard method is non-discriminatory. It will include both the crystalline and amorphous fractions of all constituents of the mixture. With the inclusion of an appropriate internal standard, the discrepancy between the mass fractions admixed during sample preparation and those obtained from the diffraction experiment indicates the total amorphous content of the mixture. In order to measure the amorphous fraction of a given sample, one can mix the sample with a material known to be completely crystalline.

Let the test sample be a mixture of crystalline phases k with mass fractions X_k ($k = 1, \ldots, n$) plus a mass fraction X_0 of amorphous material ($\sum_{k=0}^{n} X_k = 1$), and combine a unit mass of the test sample with a mass S of a purely crystalline standard which is not present in the test sample. Either RIR or QRA methods can be used to determine a set of measured crystalline mass fractions X', normalized to $\sum_{k=1}^{n} X_k{}' + X_S{}' = 1$. Then the amorphous fraction of the original sample and the original crystalline fractions are given by

$$X_0 = 1 - S\left(\frac{1}{X_S'} - 1\right) \quad \text{and} \quad X_k = X_k'(1 + S - X_0). \qquad (7)$$

This experimental method does not distinguish an amorphous surface layer from the presence of amorphous phase(s).

As noted above, the premise of this derivation, that the standard has no amorphous content, is hypothetical. However, it is applicable to the experimental design discussed in §3, where a series of Si powders are extrapolated to 100% crystallinity to establish the amorphous fraction of SRM 676a. Once the amorphous fraction, X_{0S}, of the standard has been established, equation (7) can be extended simply by substituting $S(1 - X_{0S})$ for S in (7). Thus, the provision of an appropriate standard will not only address a long-standing problem in QPA but will provide a means to evaluate powders with respect to characteristics that were previously inaccessible.

2. Alumina as an internal standard for quantitative analysis

Visser & deWolff (1964) highlighted several favorable features of corundum as a reference standard: freedom from preferred orientation, strong lines over a wide d-space range, stability, inertness, and commercial availability in the desired crystallite size. However, present-day understanding of a microstructure ideal for quantitative analysis would include some additional parameters and modify those offered by Visser & deWolff (1964). The characteristics of an ideal crystalline powder would include: strong lines over a wide d-space range, stability, inertness, equi-axial (non-orienting) particles, a particle size in the 1 μm range so as to minimize the effects of microabsorption (Brindley, 1945), and, lastly, small diffracting domains to minimize the effects of primary extinction (Zachariasen, 1945). With consideration of the amorphous content issue and the production methods for alumina, it becomes apparent that our ability to find an alumina powder appropriate for intensity measurements is somewhat fortuitous. α-Alumina is a high-temperature high-strength chemically durable ceramic that is also sufficiently tough to allow it to be utilized as a polishing and grinding medium. Given its lack of friability, obtaining the desired microstructure for QPA would have to be an integral component of the manufacturing process employed to produce the powder. While the resources available to produce a NIST SRM are significant, it is nonetheless the case that the bulk feedstock used for SRMs is almost always obtained through processes developed by industry for commercial production of large quantities. Frequently, such processes can be optimized to yield an SRM material of the desired microstructure.

The Bayer process is used to produce the majority of alumina used in ceramic applications. Wefers & Bell (1972) and Hudson (1987) describe the process and offer the 'road map' wherein aluminium trihydroxide, gibbsite, is thermally decomposed through a series of transition alumina phases to yield the commercially desired high-temperature corundum phase alumina. The microstructure of the product can be tailored during calcination with the use of mineralizers, variation of the atmosphere, heating rate and final temperature. However, these products are less than ideal as diffraction standards. Alumina powders calcined to a relatively low temperature are typically referred to as 'active' and may be of ultra-fine particle size, high surface area and equi-axial grains. However, they invariably contain phase impurities in the form of non-decomposed transition alumina phases. Alumina products that have calcined to a higher temperature are often referred to as 'tabular'. While phase-pure α-alumina, these products typically consist of coarse-grained aggregates, with the crystallites being of plate-like morphology. Comminution can be employed to address the aggregation. However, the resulting powder will display a preferred orientation, owing to a tendency for alignment of the plate-like grains.

Dynys & Halloran (1982) reported on an alternative method to produce alumina *via* the alum [$NH_4Al(SO_4)_2 \cdot 12H_2O$] precursor route. Upon thermal processing, the alum forms a sponge-like structure that persists throughout the decomposition, the sponge wall thickness determining the final particle size. The alum decomposes into the γ-phase, then directly into the corundum phase at the relatively low temperature of 1323 K. The α-phase crystallites are formed by a nucleation and growth process. A typical microstructure that results from this preparation route is illustrated in Fig. 2. With regulation of processing parameters, the wall thickness and the nucleation rate can be varied to result in the desired crystallite and particle sizes. Comminution yields particles that are fine grained, equi-axial and of high phase and chemical purity.

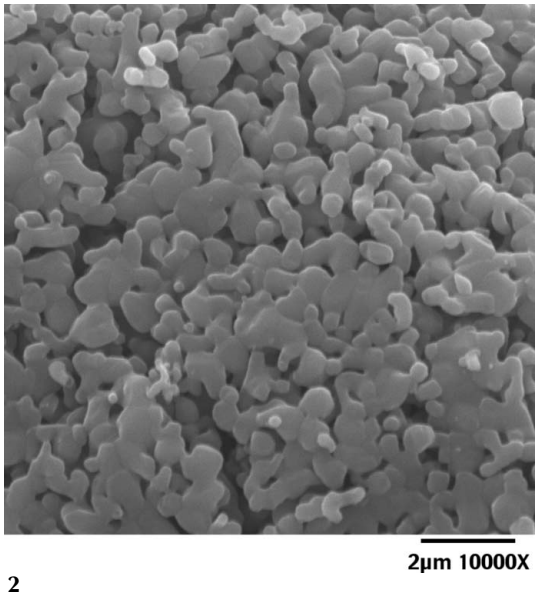

Figure 2
SEM micrograph of alum-derived corundum illustrating sponge-like microstructure.

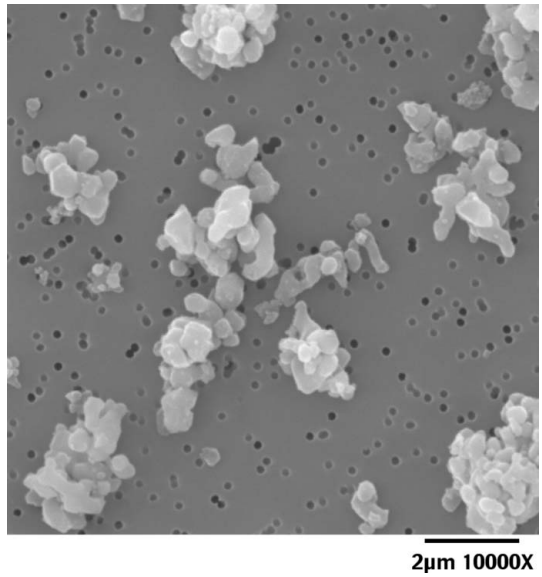

Figure 3
SEM micrograph of SRM 676a illustrating almost ideal microstructure for quantification by powder diffraction methods.

Alumina powders produced *via* this route are used in more technical applications such as the manufacture of envelopes for the high-intensity lighting industry.

The Linde[1] '*X*' series of alumina polishing compounds were manufactured in this manner. Prior to the certification of SRM 676, Linde C has been used consistently by the diffraction community for quantitative analysis since the mid-1970s. A scanning electron microscope (SEM) examination of Linde C indicated that it consisted of aggregates of $\sim$100 μm in diameter, a relic of the sponge-like precursor structure. SRM 676 consisted of Linde C that had been judiciously milled to break up the aggregates. The development of the experimental design reported in this paper began immediately after SRM 676 was certified in 1992. Early versions of such experiments indicated an impurity level of several percent, despite the fact that no impurity diffraction lines were observed in SRM 676. Gualtieri (2001) reported that the phase purity could be improved with an annealing operation. This is consistent with the presence of a small amount of a γ-alumina impurity, the highly diffuse diffraction lines of which are difficult to discern, that was transformed into corundum with annealing. It would also indicate that the calcination temperature for this product was insufficient to fully decompose the γ-phase; this, however, would not negatively influence the utility of Linde C for its intended use as a polishing compound. SRM 676 was re-certified in 2005, with a set of experiments analogous to those reported in this paper, to a phase purity of 91.75% $\pm$ 1.52%. SRM 676a (NIST, 2008) consists of Baikalox CR1, manufactured with an alum decomposition process, calcined to 1673 K, and jet milled for a de-aggregated fine-grained equi-axial phase-pure alumina powder. An SEM micrograph of SRM 676a is shown in Fig. 3, while a typical particle-size distribution determined *via* laser scattering is shown in Fig. 4.

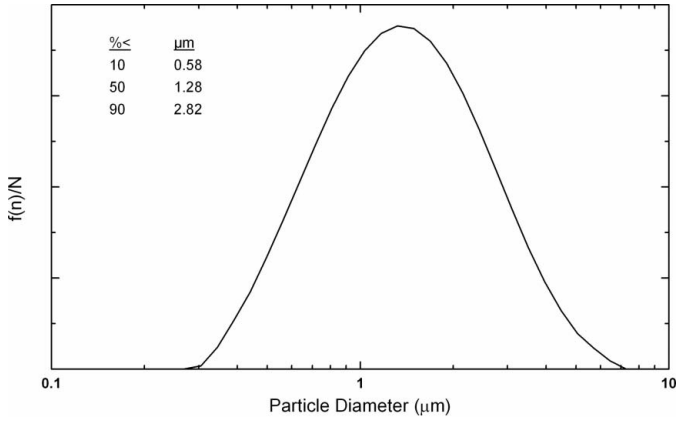

Figure 4
Typical particle size data from SRM 676a *via* laser scattering.

3. Strategy for certification of crystalline phase purity

Insofar as any crystalline powder includes an amorphous component, and since it is strongly desired to quantify its weight fraction, the current certification of SRM 676a for absolute phase purity is based on a novel procedure to quantify the amorphous material present. This was accomplished with an experiment wherein the amorphous content of a second, or reference, phase mixed with SRM 676a was varied systematically. Silicon was chosen as the reference phase for reasons that included availability, high purity, friability, and the fact that lattice defects could readily be annealed out under conditions realisable with standard laboratory equipment. Implicit in our interpretation of the data is that the

[1] Certain commercial equipment, instruments or materials are identified here in order to adequately specify the experimental procedure. Such identification does not imply recommendation or endorsement by the National Institute of Standards and Technology, nor does it imply that the materials or equipment identified are necessarily the best available for the purpose.

silicon consists of single-crystal particles with no crystallographic defects, *i.e.* that all amorphous material associated with it is confined to the crystallite surface. Furthermore, the amorphous layer thickness at the surface is assumed to be invariant with respect to crystallite size. This assumption is credible because the silicon oxide, presumed to be the chief component of any surface layer, is essentially impervious to diffusion of oxygen under ambient conditions. Given that the total surface area of a powder is inversely proportional to its particle diameter, these microstructural features permit a systematic variation of the silicon's amorphous content.

The selected silicon powder was fractionated into lots of successively larger particle sizes ranging from 5 μm to 25 μm. Mixtures of each of the lots of this silicon and SRM 676a were prepared at a 50/50 mass ratio. The mass fractions of crystalline silicon, determined *via* QRA, were then plotted relative to the specific surface area (units of $m^2\ g^{-1}$), proportional to the amorphous content, of the silicon. A successful experiment would result in the refined mass fractions of silicon successively increasing with increasing particle size. The slope of these data is determined by the amorphous layer thickness on the silicon particles. An extrapolation of these data to their infinite particle size and, therefore, zero amorphous content, would yield the mass fraction of alumina that would be determined using a hypothetical silicon powder of 100% crystalline content. Thus, the discrepancy between this mass fraction measured *via* diffraction and that of the initial weighing operation indicates the true amorphous content of the SRM 676a alumina.

The accuracy of the results is based on both the measurement of the diffraction intensity from the two phases and their accurate quantification with the Rietveld analyses. Of critical concern is the phenomenon of extinction, which will affect the diffraction intensity of the silicon owing to its large defect-free crystallite size. Such powder samples will exhibit reduced diffraction intensity owing to primary extinction. This results from the breakdown of the kinematic approximation owing to interference between the primary and diffracted beams within the domains. Secondary extinction, commonly seen in single-crystal diffraction, arises from interference from coincidently aligned mosaic blocks within a large single crystal and is thus not present in polycrystalline samples used for powder diffraction. Analytical treatments of primary extinction are available only for an infinite-slab crystal in Bragg (beam enters and exits the same face) or Laue (opposite faces) geometry. For powder samples, primary extinction can be regarded as a correction to the intensity computed from the usual kinematical diffraction theory.

The degree to which extinction affects the diffraction intensity depends upon the diffraction geometry, *i.e.* the path length of the incident and diffracted beams through each crystalline grain. Sabine (1985, 1988) developed a model for extinction, by interpolating between the results of the infinite-slab Bragg and Laue geometries. This treatment is available in closed form suitable for Rietveld refinement, and has been validated with time-of-flight (TOF) neutron measurements on MgO (Sabine *et al.*, 1988); it is implemented in the widely used Rietveld software *GSAS*.

In the Sabine theory the degree of extinction is based on a parameter x, defined as

$$x = E_x(\lambda F/V)^2, \tag{8}$$

where E_x is a refinable parameter representing the square of the coherent domain size, λ is the radiation wavelength, F is the structure factor and V is the volume of the unit cell. Larger values of x imply stronger extinction effects, *i.e.* observed intensity reduced from what would be predicted by kinematic theory. The intensity of each given reflection is reduced by a factor which depends on x and the diffraction angle 2θ; the reader is referred to Sabine (1985, 1988) for details. It is apparent from (8) that in order to realize a robust refinement of the extinction parameter one should perform an experiment over a large range of d spacings. It is also evident that the effect of extinction can be reduced by increasing the energy of radiation used, particularly for X-ray experiments.

Three of the four diffraction data sets on corundum–silicon mixtures in this work were chosen to minimize and model the effects of extinction: neutron TOF, 25 keV X-ray and 67 keV X-ray. The fourth data set was collected with Cu $K\alpha$ radiation ($\sim$8 keV); we did not address the significantly larger extinction effect with this data as the limited accessible d spacing precludes a stable refinement of the extinction parameter. However, in view of the ubiquity of laboratory powder diffractometers, comparison with the other methods is useful. Extinction lengths (essentially the size of a crystallite for which extinction is a major effect) for X-ray diffraction in Laue geometry at two Si reflections are given in Table 1 (Stepanov, 2004). The criticality of incorporating a model for extinction is indicated by correspondence between these lengths and the particle sizes of the silicon used in the experiments.

The surface character of silicon has been the subject of intense study for over 40 years owing to the critical role it plays in the operation and fabrication of semiconductor devices (Green *et al.*, 2001). An extensive discussion of the subject of the Si/SiO_2 interface can be found by Kern (1993). A virgin surface of silicon exposed to ambient laboratory conditions will oxidize in less than an hour to form a 'native' oxide layer. The kinetics of oxygen diffusion to the Si/SiO_2 interface will effectively limit the growth of the SiO_2 layer to an apparent thickness of 1.5 nm. Olsen & Shimura (1989) demonstrated that a significant portion of what was considered an oxide layer was actually adsorbed hydrocarbons. This atmospheric contamination is essentially indistinguishable from the oxide layer *via* ellipsometry methods as the density and corresponding index of refraction of the hydrocarbon layer is close to that of the SiO_2. The heating of silicon in the presence of oxygen will invariably induce further oxidation. However, during annealing at the low oxygen pressure, $P(O_2)$, used in this work, the reaction $2Si(solid) + O_2(gas) = 2SiO(gas)$ occurs, leading to a 'cleaning' of the silicon surface. Smith & Ghidini (1982) determined the critical conditions for growth *versus* removal of SiO_2 from silicon as a function of

Table 1
Instruments and parameters of the neutron and X-ray data collection.

Abbreviations: IPNS: Intense Pulsed Neutron Source, Argonne National Laboratory. NSLS: National Synchrotron Light Source, Brookhaven National Laboratory. APS: Advanced Photon Source, Argonne National Laboratory. PSD: Position-sensitive detector.

	Data sets for QPA of Si–Al_2O_3 mixtures				Data set for Al_2O_3 microstructure analysis
	Neutron TOF	Synchrotron 67 keV	Synchrotron 25 keV	Laboratory Cu $K\alpha$	Synchrotron 27 keV
Instrument	IPNS SEPD	NSLS X17B	APS 32-ID-B	Siemens D500	APS 11-BM
Monochromator	n/a	Focusing Laue Si (311)	Diamond (111)	Johansson Ge (111)	Sagittally bent Si (111)
Analyzer	n/a	Strained Laue Si (220)	Si (111)	n/a	Si (111)
Detector configuration	$\pm 144^\circ$ banks	Single	8 detectors with analyzers	Quartz wire PSD	12 detectors with analyzers
Sample size and configuration	$\sim$4 g in V can	1 mm glass capillary	0.8 mm Kapton capillary	Flat plate	0.8 mm Kapton capillary
d-spacing range (nm)	0.05–0.39	0.089–0.393	0.058–0.474	0.08–0.44	0.041–0.55
Extinction length for Si (111) (μm)		164	61	19	
Extinction length for Si (531) (μm)		336	120	21	

$P(O_2)$ and temperature. These results can be used to evaluate the impact of procedures used herein.

The Rietveld method was developed over 40 years ago for crystal structure analysis from powder diffraction data and has been applied to quantitative analysis for 20 years (Rietveld, 1969; Hill & Howard, 1987; Bish & Howard, 1988). The results are, therefore, based on robust and mature measurement technology. This experimental design also permits consistency checks through the correlation of the results from the three independent measurement devices. Furthermore, the results are constrained by physical plausibility of both the amorphous content of SRM 676a and the amorphous layer thickness of the silicon.

4. Experimental

4.1. Sample preparation

The silicon was obtained from the dedicated production run of intrinsic float-zone material that was used as the feedstock for NIST SRM 640c (NIST, 2000*a*). The boules were crushed and jet milled to yield a powder of a relatively broad size distribution. The powder was then annealed to remove microstructural defects that resulted from the comminution as per van Berkum *et al.* (1995). The quartz tube furnace used for the annealing was equipped with a mass flow controller, titanium gettering furnace, roughing vacuum pump and an oxygen sensor[2] (ZrO_2 cell) to monitor O_2 concentration in the argon gas exiting the furnace. Stainless steel tubing was used for the conduit between the gettering furnace and the tube furnace. With the furnace idling at 473 K, the sample, contained in a quartz boat, was inserted and a vacuum pulled for 5 min. The furnace was then backfilled with Ar at a flow rate of approximately 300 ml min^{-1} to result in a slight positive pressure and a final flow rate of 20 ml min^{-1}. Proper operation was assured by the oxygen sensor indicating an undetectable oxygen level in the exhaust gas, *i.e.* an O_2 concentration of less than 1 p.p.m. The evacuation/backfilling procedure was repeated immediately and after 30 min for a total of three such operations. The silicon was then heated to 1273 K for 2 h.

The silicon was then passed through a series of sieves (25 μm, 20 μm, 15 μm, 10 μm and 5 μm) as slurry in anhydrous isopropyl alcohol. The size fractions were re-washed upon the sieve defining the lower limit of its particle size to minimize any residual fine fraction. Finally, the silicon was allowed to settle out of an isopropyl alcohol slurry for 0.5 min to 20 min depending on the particle size, to remove any sub-micrometre fraction. The organic impurities from the isopropyl alcohol were removed with a wash in dilute nitric acid followed by drying. The silicon powder of SRM 640c had been prepared by jet milling to obtain a narrow particle-size distribution centered about 5 μm, and annealed by the aforementioned procedure. Microstructural data for each of the lots of silicon powder are shown in Table 2. Particle-size distributions were determined by laser scattering. The average particle diameters by mass, d_{50}, values are reported in Table 2. Specific surface area was measured by Quantachrome[3] *via* multipoint Brunauer–Emmett–Teller (BET) adsorption, using krypton as the adsorbent. Their analysis included the development of a reference material of similar specific surface area to address the uncertainty of their measurements and gave a 95% confidence ($k = 2$; Taylor & Kuyatt, 1994) uncertainty interval of ± 0.022 (m^2 g^{-1}) for the data of Table 2.

Aliquots of NIST SRM 676a corundum were taken from ten randomly chosen bottles of the population of $\sim$500 for this certification. Si from each of the six lots described in Table 2 was weighed and mixed with the corundum, for a total of 24 specimens of 4 g each, with nominal 50/50 mass ratio. With these fine powders, weighing is complicated by contact forces that induce adherence of the fine grains onto the weighing paper. Therefore, a separate piece of weighing paper was used for the two phases of each sample. By weighing the paper both before and after weighing the sample, the actual mass of material added to the mix can be determined. The actual Si weight fraction (population average $\pm$ standard deviation = 0.49997 $\pm$ 0.00008) was recorded for each sample, and

[2] Model S-3A, AEI Technologies, 520 East Ogden Avenue, Naperville, IL 60563, USA.

[3] Laboratory Services, Quantachrome Instruments, 1900 Corporate Drive, Boynton Beach, FL 33426, USA.

Table 2
Microstructure data from the five lots of silicon and SRM 640c.

	Sieve fraction					
	<5 μm	SRM 640c	5 to <10 μm	10 to <15 μm	15 to <20 μm	20 to <25 μm
Particle size, laser (μm)	5.28	4.44	9.81	14.47	19.24	23.98
Specific surface area, BET ($m^2\ g^{-1}$)	1.50	1.40	0.70	0.41	0.31	0.27

subsequent data analysis included a correction for this deviation. The weighing process had an estimated uncertainty of ±20 μg in each mass, which in turn leads to an uncertainty of the Si mass fraction of $\pm 7 \times 10^{-6}$, significantly less than uncertainties from the X-ray measurements.

4.2. Data collection

Data sets of the 50/50 mixtures of Si and SRM 676a corundum were measured on four instruments: neutron TOF, synchrotron beamlines operating at nominally 67 keV and 25 keV, and a laboratory diffractometer with Cu $K\alpha$ radiation. Additional measurements of SRM 676a and SRM 660a (NIST, 2000*b*) LaB_6 were made for the purpose of microstructure analysis with synchrotron radiation at 27 keV. Details of instruments and data ranges are given in Table 1. The run order of samples was separately randomized on an informal basis for all data collections. The samples were spun during the synchrotron X-ray measurements in order to ensure that a statistically large number of grains were illuminated at each point in each data set, obviating any concern over particle sampling statistics within the gauge volume.

4.3. Data analysis

The Rietveld analyses of the mixtures were performed using *GSAS* with the *EXPGUI* interface (Toby, 2001). All 24 specimens were simultaneously refined in four independent refinements, one for each diffraction instrument. The lattice parameter of Si was fixed to the certified values of SRM 640a in all refinements. Within the 24 histograms refined on each instrument, the following parameters were constrained to be equal: profile-shape terms for corundum and for each of the six lots of Si, corundum atomic parameters, thermal parameters of each phase, strain broadening and anisotropic particle shape of the corundum (which were absent in the Si), and the Sabine (1985) extinction parameter for each Si fraction. In the neutron TOF refinement the absorption term was constrained to a single value throughout. The diffractometer parameters affecting peak position were independently refined for each of the 24 histograms in each refinement to allow for small variations of effective sample position (neutrons) and instrumental shifts of wavelength and zero angle (X-rays). The background of each diffraction pattern was fitted by an eighth-order shifted Chebyshev polynomial. TOF profile function 3 and CW profile function 3 within *GSAS* were used to fit the data. Representative fits from all four instruments of the same (20–25 μm) Si fraction are shown in Fig. 5.

The laboratory X-ray data were analyzed with the intention of determining whether the Sabine extinction correction was applicable to samples measured here, rather than to obtain an independent measure of amorphous fraction of SRM 676a. Analysis of the laboratory data was performed largely as per Cline (2000). The pressing operation used for sample mounting evidently caused preferential orientation of the silicon in the 111 direction. These effects were addressed using the March (1932)–Dollase (1986) model. The model was used independently for each sample; the average of the r values (r = 1 for no preferred orientation) realized for each lot ranged from 0.72 to 0.57 with increasing particle size. Upon completion of the refinement, the extinction parameters of the four coarser fractions of silicon were manually adjusted to realize phase fractions that straddled those obtained with the other two X-ray diffraction experiments. In order to gauge the importance of the extinction correction in the other data sets, a set of fits was also performed with the extinction parameter set equal to zero.

The microstructure of SRM 676a was studied in independent measurements of that material alone. Deconvolution of the sample broadening function from the observed data was performed using *TOPAS*.[4] First, the instrumental profile function (IPF) was determined *via* profile fitting of SRM 660a (LaB_6) data using the pseudo-Voigt profile function with sample FWHM terms constrained to be constant with 2θ. Two 'circles' functions with a $\tan(\theta)$ dependence were included to model the slight profile asymmetry. One was constrained to be negative to fit the low-angle feature, while the other was positive for fitting of the high-angle asymmetry. With that IPF, broadening of SRM 676a was found to be entirely Lorentzian in nature, with the 'microstrain', $\tan(\theta)$, component being insignificant. *TOPAS* was programmed to compute the volume- and area-weighted dimensions. Those parameters were used to derive a presumed log-normal crystallite size distribution (Fig. 6), according to the method of Krill & Birringer (1997), using equations presented by Popa & Balzar (2002) and implemented by Whitfield (2006).

5. Results and discussion

The refined mass fractions of Si were determined from the data of the neutron TOF, 25 keV and 67 keV X-ray powder diffraction measurements. These are shown in Fig. 7 as a function of specific surface area. As discussed above, the data were corrected individually for the measured Si weight fractions, and the fits were performed with refined values of the

[4] V4.2, Bruker AXS GmbH, Karlsruhe, Germany.

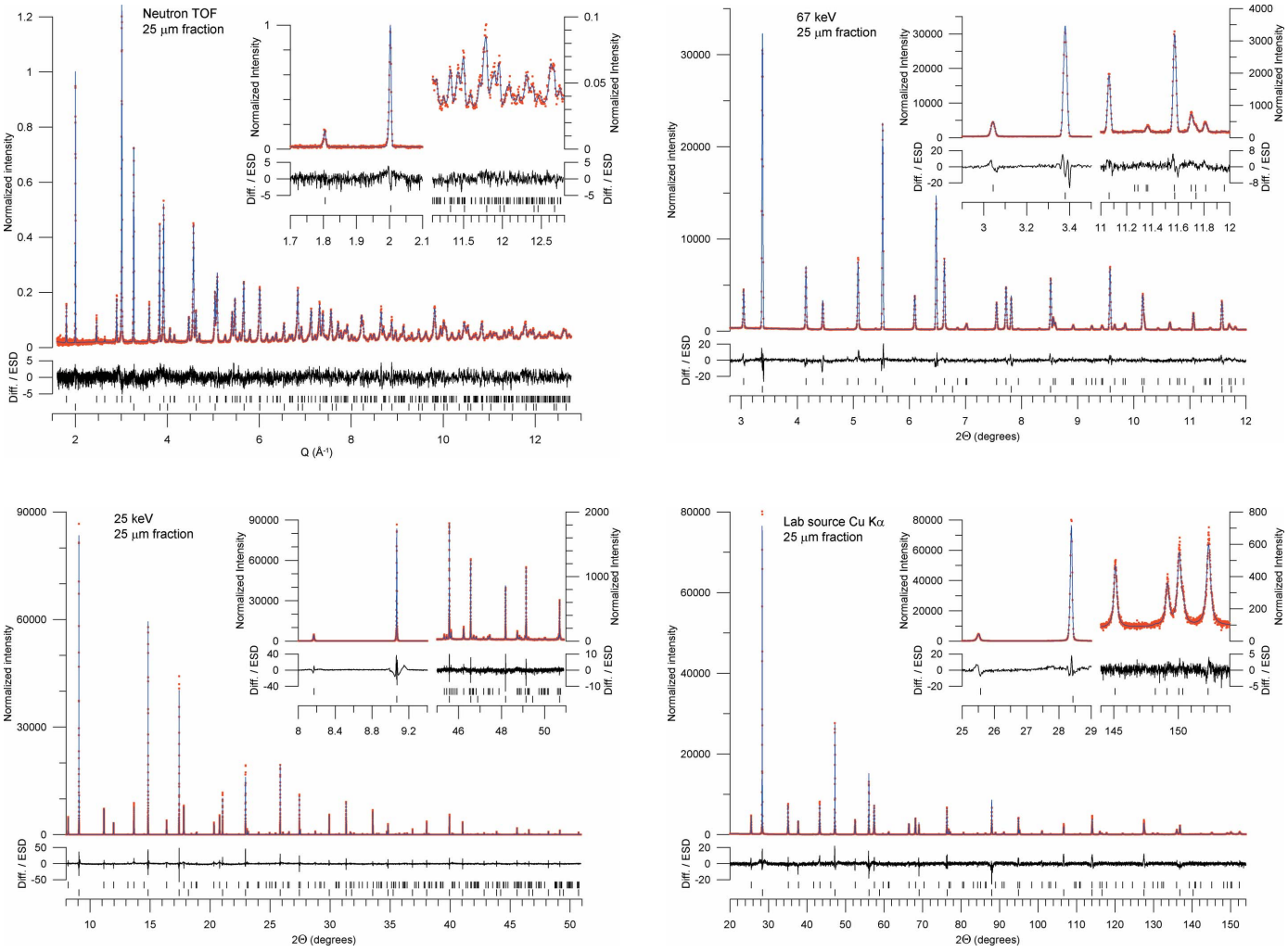

Figure 5
Rietveld fits of the 20–25 μm Si fraction from each of the four instruments used in the QPA.

extinction parameter. All data sets illustrate a reduction in the refined mass fraction of silicon as its surface area increases, consistent with the expectation of the experimental design. Results from a linear least-squares fit to the Si mass fraction *versus* silicon surface area from each independent set of measurements are given in Table 3. Refinements were also performed without the extinction correction, and those results are presented in Fig. 8. As expected, removal of the extinction

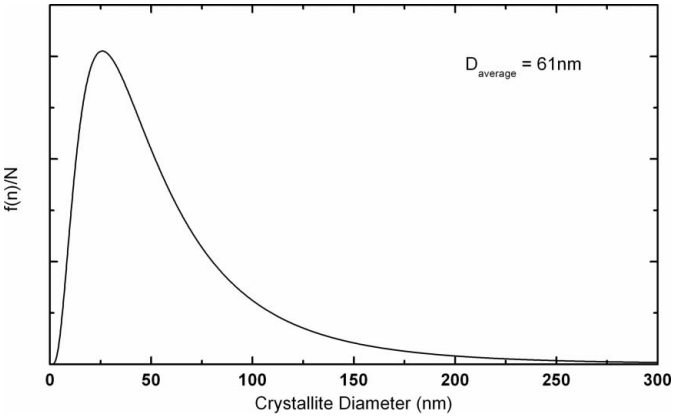

Figure 6
Crystallite size distribution, presumed log-normal of SRM 676a determined *via* profile shape analysis.

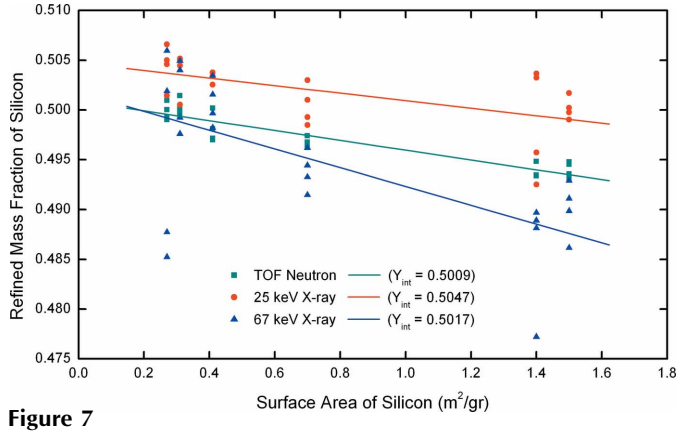

Figure 7
Values of refined mass fraction of silicon *versus* specific surface area of silicon for the neutron TOF and 25 and 67 keV X-ray data, corrected for extinction. Linear fits and values to each of the three data sets are also shown.

Table 3
Results from linear least-squares fits of the data of Fig. 7.

	Neutron TOF	25 keV X-ray	67 keV X-ray
y intercept	0.5009	0.5047	0.5017
$SD_{intercept}$	0.00039	0.00099	0.00208
Slope	−0.00494	−0.00378	−0.00943

correction led to lower estimated mass fractions of Si for the larger Si grain sizes, enough so that none of the data sets supports a linear extrapolation to low specific surface area.

The Rietveld refinements give estimated standard uncertainties of the phase fractions which are of the order of the size of the symbols in Figs. 7 and 8. These reflect the contribution of counting statistics alone, propagated through the least-squares fitting procedure. It is well known that the precision of parameters derived from Rietveld fits are generally poorer than the statistical uncertainties derived from the fit, and so it is not surprising to find scatter among the derived mass fractions that is significantly larger than the standard uncertainty of each measurement. This indicates that causes of the distribution in these data are non-statistical in nature. The origin of the scatter of the refined mass fractions of identically prepared samples is not obvious. However, it is in general accord with previous work on reproducibility of QPA by Rietveld refinement (Madsen *et al.*, 2001). The relatively small gauge volume of sample used in the X-ray experiments was cause to consider these data for the effects of particle counting statistics. The spread in the four data points, however, from the fine to the coarse fractions is observed to be largely uniform; this is consistent with the conclusion that the effect of particle counting statistics are not operative on these data.

A closer evaluation of the data indicate that, while there are differences in slope and position between the three data sets, each data set is self-consistent, and conforms with the expectations of the experimental design. Furthermore, a Grubbs (1969) test indicated that each data set contained no statistical outliers. Refined parameters that characterized crystal structure, microstructure and instrumentation were all consistent

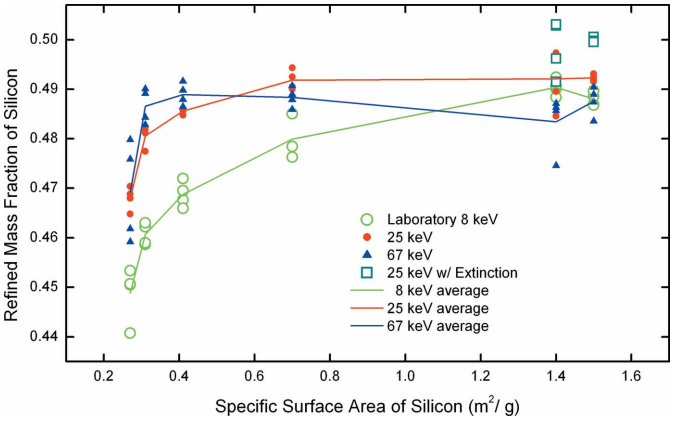

Figure 8
Values of refined mass fraction of silicon obtained for X-ray data sets analyzed in the absence of the extinction model, except for the two finer grain sizes of the 25 keV data for which the extinction model was included.

with published or plausible values. Therefore, all three data sets of Fig. 7 were used to determine the certified values and their error bounds with equal weighting. The y intercept values from the linear fits for the three diffraction techniques were averaged to yield $\bar{y} = 0.50245$.

In the notation of equation (7), where the standard is a hypothetical sample of silicon with negligible amorphous content, and $S = 1$,

$$\bar{y} = \frac{X'_{Si}}{X'_{Si} + X'_{SRM676a}} \Rightarrow X_0 = 1 - 1 \times \left(\frac{X'_{SRM676a}}{X'_{Si}}\right) = 2 - (\bar{y})^{-1} = 0.00975. \quad (9)$$

This is the main experimental result from this work. Extrapolated to negligible amorphous content of Si, a 50/50 weight mixture of Si and SRM 676a corundum is missing about 1% of the crystalline corundum, *i.e.* SRM 676a has an amorphous content of the order of 1%. The remainder of this paper is devoted to establishing a confidence interval for that number, and interpretation of the results.

Two procedures for estimating the standard deviation of the mean, $SD(\bar{y})$, were utilized. The first ignored the standard deviation of the intercept ($SD_{intercept}$) value from each linear fit and treated each of the three intercept values as raw data; this approach is appropriate when the values differ significantly. The standard deviation of the three values was 0.0020076, leading to a standard deviation of the mean smaller by a factor of $3^{-1/2}$: $SD(\bar{y}) = 0.0011590$.

The second estimate was computed by making use of the standard deviations of the individual intercepts; this approach is appropriate when the three values being combined do not differ drastically, as was the case here,

$$\begin{aligned} SD(\bar{y}) &= SD\left(\frac{y_1 + y_2 + y_3}{3}\right), \\ SD(\bar{y}) &= \frac{1}{3}\left[\mathrm{Var}(y_1) + \mathrm{Var}(y_2) + \mathrm{Var}(y_3)\right]^{1/2}, \\ SD(\bar{y}) &= 0.00077879. \end{aligned} \quad (10)$$

Although justification exists for choosing the latter method, a more conservative statistical approach, which provides further protection from unforeseen sources of variation, is to utilize the results from both methods in a root-mean-squares fashion to yield a final value for $SD(\bar{y})$,

$$\begin{aligned} SD(\bar{y}) &= \left\{\left[SD(\bar{y}_{proc1})\right]^2 + \left[SD(\bar{y}_{proc2})\right]^2\right\}^{1/2}, \\ SD(\bar{y}) &= \left(0.0011590^2 + 0.00077879^2\right)^{1/2}, \\ SD(\bar{y}) &= 0.0013964. \end{aligned} \quad (11)$$

It is evident from equation (9) that the standard deviation of X_0 may be computed as

$$SD(X_0) = \frac{SD(\bar{y})}{(\bar{y})^2} = 0.00553. \quad (12)$$

Using an expanded uncertainty coverage factor of $k = 2$, (ISO, 1993; Taylor & Kuyatt, 1994), the final value for the certified phase purity of SRM 676a is therefore 99.02% ± 1.11%. Even

though a phase purity greater than 100% is a physical impossibility, the statement that the expanded uncertainty interval includes values above 100% is perfectly reasonable.

The slope of the line fit through the silicon mass fractions of the 67 keV data is roughly twice that of either of the other two methods, while a simple offset separates the neutron TOF and 25 keV data. This project started with the 67 keV experiment, in the expectation that results would be free of extinction effects, *i.e.* that the radiation was of such short wavelength that extinction would be negligible. Hence, data for this experiment were collected over a relatively limited *d*-space range; inclusion of the extinction correction was presumed unnecessary. With analysis of the data, however, the need to refine the extinction domain sizes became apparent. This result points to the necessity of further work, both experimental (more complete measurements at short wavelength) and theoretical (better model for extinction in powders).

The data of Fig. 8 illustrate the silicon mass fractions determined *via* X-rays with the extinction correction omitted. The reduction in refined mass fractions of the coarse particle sizes of silicon follow the expected wavelength and particle-size dependence. However, with the smaller size fractions, a correspondence in all three data sets is noted. Observing the disparity between these data and those from the 25 keV experiment with the extinction correction, one concludes that extinction effects are operative even in the fine-grained 5 µm region for all radiation energies used.

Consideration of these observations indicates that there is neither a domain size nor diffraction energy threshold for the effects of extinction. This observation emphasizes the criticality of the small domain size requirement for a quantitative analysis standard. The data of Fig. 6 illustrate the domain size distribution (assumed to be log-normal) of SRM 676a determined through a profile-shape analysis. The analysis indicates an average particle diameter of 61 nm and quite a broad distribution, not unexpected given the manufacturing process. While the uncertainties of the numerical aspects of these data are quite large, this crystallite size distribution is nonetheless conclusive in indicating that the alumina of SRM 676a will not display the adverse effects of extinction. One would prefer a more narrow distribution centered in the 100 nm region; however, it is not likely that one can further customize the alumina production process to realize a more optimal microstructure for future renewals of SRM 676.

Some additional observations: the data of the neutron TOF experiments are the most uniform, followed by that of the 25 keV, while that of the 67 keV displays the widest distribution. That the 67 keV data display the greatest level of noise is not unexpected given the limited *d*-space range of these data. The March–Dollase parameter refined to correct for the 111 preferred orientation of the silicon in the laboratory data varied from 0.72 to 0.57 with increasing particle size. The refined extinction domain sizes are plotted relative to particle size as determined *via* laser scattering, Table 2, in Fig. 9. The values shown for the 8 keV laboratory X-ray data were determined by manually adjusting them as previously described. The error bars shown reflect a 2σ value determined

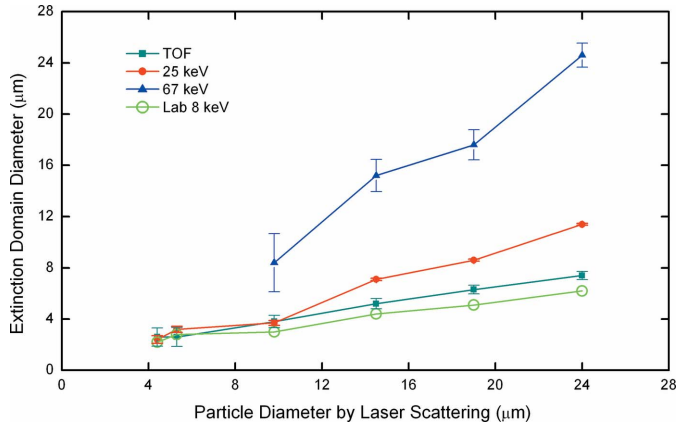

Figure 9
Extinction domain sizes refined for the TOF, 25 and 67 keV X-ray data, manually set for the laboratory 8 keV data. Error bars represent 2σ values obtained from the ESDs of the refinements.

from the ESDs of the refined extinction parameters. A lack of correspondence in the refined extinction domain sizes for the silicon is noted between the diffraction methods. However, trends within methods are self-consistent. While the sizes shown for the 67 keV data appear in close correspondence with the particle-size data, they are regarded as the least credible as the domain size is certainly far less than the particle size owing to low-angle grain boundaries presumed present from the comminution process used to prepare the powder.

Based on Smith & Ghidini (1982) with respect to the annealing temperature and O_2 concentration of this work, the silicon was cleaned of the excess oxide layer at the conclusion of the anneal. The native oxide layer would of course reform when the silicon was re-exposed to ambient laboratory conditions. Therefore, we evaluate the slope of the data of Fig. 7 to compute the amorphous layer thickness on the silicon with the expectation that the result will be consistent with a 'native' oxide thickness. While previous discussions offer that the slope of the 67 keV data is excessive, we proceed with the average slope from all data sets, -0.0061 g m^{-2}.

Uemura *et al.* (2001) reported grazing-incidence X-ray reflectometry measurements that indicated that the density of SiO_2 grown on silicon in air was 2.1 g cm^{-3}, considerably less than the bulk value of 2.5–2.65 g cm^{-3} for quartz. We use a value of 2.2 g cm^{-3}. Then, the amorphous layer thickness is obtained as the slope divided by the density, which yields a value of 2.8 nm. This is somewhat in excess of reported values, but not unreasonable.

6. Conclusions

SRM 676a consists of alumina powder possessing a microstructure demonstrated to be almost ideal for quantification measurements *via* powder diffraction methods. The only material other than crystalline corundum present is amorphous, and the 95% confidence limits for amorphous content are from zero to 2.1%. The results of the experiments presented converge upon a credible certification of SRM 676a

for its amorphous content. This certification allows the determination of amorphous content in QPA.

The disparities in the data among the three sets of diffraction measurements described are non-statistical in nature and remain unexplained. They are, however, small in absolute magnitude. The neutron TOF data yield results with the greatest internal consistency; the data covered the largest *d*-space range and were most amenable to addressing the effects of extinction *via* the Sabine (1988) model as implemented in *GSAS*. The 67 keV X-ray data produced the broadest distribution in results. This is presumably due to the limited *d*-space range sampled in these data that prevented an effective refinement of the extinction parameter. Extinction effects were observed at 67 keV and with crystallite sizes of less than 5 μm. This effect should be considered with regard to all quantitative phase analysis experiments on highly crystalline materials.

We are grateful to the following individuals: Marty Green of the NIST Ceramics Division, Material Science and Engineering Laboratory for discussions concerning the surface character of silicon; Ashfia Huq of Oak Ridge National Laboratory for early contributions to this project leading to the re-certification of SRM 676 for amorphous content; Peter L. Lee for the collection of 25 keV data on beamline 32-ID-B at the Advanced Photon Source; Max Peltz of the NIST Materials and Construction Research Division, Building Fire and Research Laboratory, for the collection of the light scattering particle-size data; Brian Toby for useful discussions; and Pamela Whitfield of National Research Council, Canada, for assistance with the computations concerning the crystallite size distribution of SRM 676a. Use of the Advanced Photon Source and Intense Pulsed Neutron Source was supported by the US Department of Energy, Office of Science, Office of Basic Energy Sciences, under contract No. DE-AC02-06CH11357. Use of the National Synchrotron Light Source, Brookhaven National Laboratory, was supported by the US Department of Energy, Office of Science, Office of Basic Energy Sciences, under contract No. DE-AC02-98CH10886.

References

Berkum, J. G. M. van, Sprong, G. J. M., de Keijser, Th. H., Delhez, R. & Sonneveld, E. J. (1995). *Powder Diffr. J.* **10**, 129–139.
Bish, D. L. & Howard, S. A. (1988). *J. Appl. Cryst.* **21**, 86–91.
Brindley, G. W. (1945). *Philos. Mag.* **36**, 347.
Chung, F. H. (1974*a*). *J. Appl. Cryst.* **7**, 519–525.
Chung, F. H. (1974*b*). *J. Appl. Cryst.* **7**, 526–531.
Cline, J. P. (2000). *Industrial Applications of X-ray Diffraction*, edited by F. H. Chung & D. K. Smith, pp. 903–917. New York: Marcel Dekker.
Dollase, W. A. (1986). *J. Appl. Cryst.* **19**, 267–272.
Dynys, F. W. & Halloran, J. W. (1982). *J. Am. Ceram. Soc.* **65**, 442–448.
Green, M. L., Gusev, E. P., Degraeve, R. & Garfunkel, E. L. (2001). *Appl. Phys. Rev.* **90**, 2057–2121.
Grubbs, F. (1969). *Technometrics*, **11**, 1–21.
Gualtieri, A. F. (2001). Personal communication.
Hill, R. J. & Howard, C. J. (1987). *J. Appl. Cryst.* **20**, 467–474.
Hudson, L. K. (1987). *Production of Aluminium and Alumina*, pp. 11–46. New York: John Wiley and Sons.
ISO (1993). *Guide to the Expression of Uncertainty in Measurement*, 1st ed. Geneva: International Organization for Standardization.
Kern, W. (1993). *Handbook of Semiconductor Wafer Cleaning Technology*. Park Ridge: Noyes.
Klug, H. P. & Alexander, L. E. (1974). *X-ray Diffraction Procedures*, 2nd ed. New York: John Wiley and Sons.
Krill, C. E. & Birringer, R. (1997). *Philos. Mag.* **77**, 621–640.
Larson, A. C. & Von Dreele, R. B. (2004). *General Structure Analysis System*. Report LAUR 86–748. Los Alamos National Laboratory, NM, USA.
Madsen, I. C. & Scarlett, N. V. Y. (2008). *Powder Diffraction Theory and Practice*, edited by R. E. Dinnebier and S. J. L. Billinge. Cambridge: Royal Society of Chemistry Publishing.
Madsen, I. C., Scarlett, N. V. Y., Cranswick, L. M. D. & Lwin, T. (2001). *J. Appl. Cryst.* **34**, 409–426.
March, A. (1932). *Z. Kristallogr.* **81**, 285.
NIST (2000*a*). Standard Reference Material 640c. NIST, Gaithersburg, MD, USA (https://www-s.nist.gov/srmors/view_detail.cfm?srm=640C).
NIST (2000*b*). Standard Reference Material 660a. NIST, Gaithersburg, MD, USA (https://www-s.nist.gov/srmors/view_detail.cfm?srm=660A).
NIST (2005). Standard Reference Material 676. NIST, Gaithersburg, MD, USA (https://www-s.nist.gov/srmors/view_detail.cfm?srm=676).
NIST (2008). Standard Reference Material 676a. NIST, Gaithersburg, MD, USA (https://www-s.nist.gov/srmors/view_detail.cfm?srm=676A).
Olsen, J. E. & Shimura, F. (1989). *J. Vac. Sci. Technol. A*, **6**, 3275–3278.
Popa, N. C. & Balzar, D. (2002). *J. Appl. Cryst.* **35**, 338–346.
Rietveld, H. M. (1969). *J. Appl. Cryst.* **2**, 65–71.
Sabine, T. M. (1985). *Aust. J. Phys.* **38**, 507–518.
Sabine, T. M. (1988). *Acta Cryst.* A**44**, 368–374.
Sabine, T. M., Von Dreele, R. B. & Jørgensen, J.-E. (1988). *Acta Cryst.* A**44**, 374–379.
Smith, F. W. & Ghidini, G. (1982). *J. Electrochem. Soc.* **129**, 1300–1306.
Snyder, R. L. (1992). *Powder Diffr. J.* **7**, 186–192.
Stepanov, S. A. (2004). *Proc. SPIE*, **5536**, 16–26.
Taylor, B. N. & Kuyatt, C. E. (1994). Technical Note 1297. NIST, Gaithersburg, MD, USA (http://physics.nist.gov/Pubs).
Toby, B. H. (2001). *J. Appl. Cryst.* **34**, 210–213.
Uemura, S., Fujii, M., Hashimoto, H. & Nagai, N. (2001). *Jpn. J. Appl. Phys.* **40**, 5312–5313.
Visser, J. W. & deWolff, P. M. (1964). Report No. 641.109. Technisch Physische Dienst, Delft, The Netherlands.
Wefers, K. & Bell, G. M. (1972). Technical Paper No. 19. Alcoa Research Laboratories, New Kensington, PA, USA.
Whitfield, P. (2006). Presented at the *1st TOPAS User Meeting*, Denver, CO, USA; and personal communication.
Zachariasen, W. H. (1945). *Theory of X-ray Diffraction in Crystals*. New York: Dover.